CrossMark

RESEARCH PAPER

Three-dimensional hydrodynamic flow focusing of dye, particles and cells in a microfluidic device by employing two bends of opposite curvature

Siddhartha Tripathi[1] · Amit Kumar[1] · Y. V. Bala Varun Kumar[1] · Amit Agrawal[1]

Abstract This work relates to three-dimensional (3D) hydrodynamic flow focusing, wherein sample is encapsulated by sheath fluid in all the directions, making it a preferred method for particle focusing. Given the complex phenomenon involved in achieving 3D hydrodynamic focusing, we have been able to demonstrate a relatively simple microdevice for achieving this objective. In this work, a novel approach for 3D focusing utilizing two bends of opposite curvature in microchannel is proposed and demonstrated through experiments and numerical simulations. The proposed microdevice is fabricated on a single layer of polydimethylsiloxane and a single sheath inlet is used, thereby simplifying the 3D focusing mechanism and reducing the requirements of cost enhancing accessories. The mechanism underlying particle focusing is examined in detail. This microdevice provides several distinct advantages over other designs mentioned in the literature.

Keywords Three-dimensional hydrodynamic focusing · Secondary flow · Microchannel · Confocal microscopy · Discrete particle model-based simulation

List of symbols
h Height of the microchannel
w Width of the microchannel
u_s Sample velocity
u_{sh} Sheath velocity
u_p Velocity of the particle
u Velocity of fluid

U_D Dean drag velocity
d_p Diameter of particle
D_h Hydraulic diameter of microchannel
Re   Reynolds number
Re_f Reynolds number of the fluid
De   Dean number
R_c Mean radius of curvature of the microchannel
ρ_p Particle density
ρ_f Fluid density
μ_f Fluid viscosity
F_{centg} Net centrifugal force
F_{netg} Net gravitational force
F_D Drag force
F_L Net lift force
y_m^* Normalized mean lateral position along width
z_m^* Normalized mean lateral position along height
y_σ^* Normalized standard deviation along width
z_σ^* Normal standard deviation along height
H Helicity
V Velocity vector

✉ Amit Agrawal
   amit.agrawal@iitb.ac.in

[1] Department of Mechanical Engineering, Indian Institute
    of Technology Bombay, Powai, Mumbai 400076, India

1 Introduction

The aim of hydrodynamic flow focusing is to focus the sample fluid using a sheath fluid. Hydrodynamic focusing is a simple yet effective technique for flow focusing and control. It has been successfully utilized in various microfluidic applications. This includes on-chip microfluidic flow cytometry (where hydrodynamic flow focusing is used to focus the cells suspended in the sample fluid in a single file, which can then be utilized for counting/sorting of cells; Lee et al. 2001a; Chung et al. 2003; Lee et al. 2005), flow switches (for injection of sample in the desired outlet port by controlling the sheath flow rate; Lee et al. 2001b),

liquid–liquid optical waveguides (Brown et al. 2006), health monitoring (measuring ATP from erythrocytes; de Mello and Edel 2007), generation of microdroplets (Anna et al. 2002), and micromixers (Knight et al. 1998). It has also been used in micro-PIV to aid in improving the performance by concentrating the seeding traces into a thin sheet (Blonski et al. 2011).

Hydrodynamic focusing can be 2D (two-dimensional) or 3D (three-dimensional). In 2D focusing, the sample fluid is compressed/sandwiched only in one direction (the horizontal direction) by the two side flowing sheath fluids; this results in a thin sheet of sample extending downstream along the depth of the microchannel (Knight et al. 1998; Stiles et al. 2005; Lee et al. 2006; Tripathi et al. 2014). However, 3D focusing allows for sample being completely surrounded with sheath fluid in all directions, and this is realized by compressing the sample flow in both the horizontal and vertical directions (Sundararajan et al. 2004; Simonnet and Groisman 2006; Chang et al. 2007; Mao et al. 2007; Howell et al. 2008; Kennedy et al. 2009; Mao et al. 2009; Lee et al. 2009; Lin et al. 2012; Ha et al. 2014). This enables better detection of sample/particles and makes 3D focusing the preferred way of sample focusing. 3D focusing also resolves contamination issues and results in lower sample consumption. An approach to achieve 3D focusing would be to inject the sample fluid with a small diameter tube at the center of a larger tube containing the sheath flow, i.e., a centerline injector. This works considerably well at the macroscale. However, to replicate this at microscale involves considerably complex fabrication techniques. Therefore, achieving complete 3D focusing, especially at microscale, appears challenging and has been an area of active research in recent times. Although 3D hydrodynamic focusing has been achieved in few microdevices, the fabrication process is either too complicated and/or multiple sheath fluids are used to achieve focusing. Some groups have reported simplified versions of microdevices which can effectively focus the sample/particles in three dimensions using planar structure (Mao et al. 2007; Mao et al. 2009; Lee et al. 2009; Lin et al. 2012; Ha et al. 2014). But there certainly seems to be further scope to realize a microdevice which can provide the desired result of 3D sample focusing in a cost effective manner.

Several researchers have adopted diverse approaches to accomplish the goal of 3D hydrodynamic flow focusing. Amini et al. (2013) have presented various approaches using sequenced microstructures to obtain any desired shape of the fluid stream. Sundararajan et al. (2004) reported a microfluidic device capable of sample focusing in both horizontal and vertical directions. Their design required six sheath inlets and multilayer structure to achieve focusing. The design of Simmonet et al. (2006) is a high-throughput microdevice capable of streaming the cells/particles in three

dimensions. Their microfluidic device has four inlets and one outlet, and fabrication requires a multilayer process. Chang et al. (2007) reported a 3D hydrodynamic flow focusing microdevice comprising two PDMS layers, four inlet ports and one outlet port. In this device, the sample is first vertically focused using two sheath flows and then horizontally focused using sheath in cross-flow. This device works well only at low Reynolds number. Kennedy et al. (2009) reported a 3D hydrodynamic flow focusing microdevice comprising two complementary pieces of PDMS aligned to form the device. The device comprises four sheath inlets and is capable of focusing the sample in two stages. Most of these microdevices involve complicated fabrication procedures and employ multisheath inlets, resulting in additional requirements for pumping.

Mao et al. (2007) reported a 3D hydrodynamic flow focusing device which was capable of focusing the sample by inducing secondary flows in the microchannel with the use of single layer of PDMS. They named the focusing technique as "microfluidic drifting." Later on, they demonstrated this capability on-chip microfluidic flow cytometer by focusing cells resembling human CD4 + T lymphocyte cells (Mao et al. 2009). However, they used two sheath inlets resulting in the requirement of three pumps for the system. Lee et al. (2009) invented a 3D focusing device based on single layer of PDMS and single sheath inlet. Their design used Dean vortices along with contraction–expansion array for flow focusing, which was achieved at the fourth contraction region. However, the design was limited by low throughput and difficulty in controlling the sample flow. Lin et al. (2012) presented a three-dimensional focusing device which was also based on single-layer PDMS and single sheath inlet configuration. The novel approach employed in this design was to make the diameter of the sheath inlet larger than the microchannel, and under specific flow conditions, flow focusing was achieved. However, an additional step of bonding the PDMS layer is required in the fabrication process. Recently, Ha et al. (2014) reported a device capable of focusing the sample in three dimensions in a curved microchannel. The design makes use of four Dean vortices, and it works well only at high flow rates, thereby requiring additional systems for its continuous operation; also the sample is not fully focused at the center of the microchannel.

Howell et al. (2008) reported "stripe-based" and "chevron-based" designs utilizing grooves in the microchannel to accomplish 3D focusing of sample fluid. The stripe-based design uses single inlet for sheath, whereas the chevron-based design uses two inlets for the sheath fluid. Paiè et al. (2014) present a femtosecond-laser-fabricated microfluidic channel, capable of focusing the sample in 2D and 3D. The design employs two flow inlets, one for sample and other for sheath. Though the design appears to be very

interesting, the fabrication technique employed may pose challenges. Chiu et al. (2013) designed a two-layer microfluidic device which can confine particles/beads in three dimensions by varying the depth of sample and sheath microchannels; the major advantage of their design is tight confinement of sample along the centerline of the microchannel with lower control volumes, and it does not require any sophisticated visualization equipment to characterize 3D focusing.

The above microdevices have one or more of the following disadvantages: They involve complicated fabrication such as multiple photolithography steps. Some of these devices comprise multiple sheath inlets, thereby requiring additional pumping arrangements. Most of the devices also suffer from low throughput and have difficulty in controlling and centering the sample flow. They often require additional systems and devices for continuous operation, thereby increasing operational cost, and work in certain specific range of flow rates (or Reynolds number) only. These issues motivated us to explore better designs for three-dimensional hydrodynamic flow focusing.

The design presented in this work is based on controlling and utilization of secondary flows generated due to curvature effects. The device is fabricated with a single layer of PDMS, and two curvatures/bends are effectively exploited to obtain focusing with a single sheath inlet. Numerical simulations were carried out for designing the microdevice. To the best of our knowledge, two opposite bending curves have been employed to achieve 3D focusing for the first time. The design is validated through experiments with dye, particles and also with human blood cells. The simulation results are well substantiated with the experimental findings. The major advantages of the proposed design are its simple structure, ease in fabrication, and use of a single sheath inlet amongst others, such as the centralized positioning of sample flow, and sample control.

2 The proposed 3D hydrodynamic flow focusing device

The design of the proposed 3D hydrodynamic flow focusing device is illustrated through Fig. 1. The microdevice (width 200 μm × depth 100 μm) has two inlets (one each for sample fluid and sheath fluid) and one outlet. The microdevice essentially comprises of two curves, besides certain straight channel segments. The first curve is used to focus the sample in the vertical direction (top and bottom wall of the microchannel), and the second curve is used for horizontal focusing/centering the sample (inner and outer side wall of the microchannel). The inner radius of curvature is 200 μm and outer radius of curvature is 400 μm along Curve 1 and Curve 2.

The basic idea behind this design formulation is the exploitation of secondary forces generated owing to curvature effects which leads to vertical focusing of the sample fluid. Further, centrifugal forces can be brought into action by providing an additional curve which leads to horizontal focusing of the sample. However, the radius of curvature of the bends and their included angles need to be carefully chosen in order to fully exploit the above-mentioned effects.

3 Materials and methods

This section provides details about the fabrication of the microchannel, experimental setup and detection methods employed. Details about numerical simulations are also provided in this section.

3.1 Fabrication of the microchannel

A standard two-inch silicon wafer was used as the starting substrate. Conventional lithography technique, i.e., a combination of photolithography and soft lithography was employed to fabricate the microchannels. A schematic of the microchannel design is shown in Fig. 2a. A photograph of the final, ready-to-use PDMS microdevice is also shown in Fig. 2b. The entire fabrication was done in-house. The width of the microchannel was kept at 200 μm (±3 μm), and the depth of the microchannel was 100 μm (±5 μm).

Here, we present a brief overview of the fabrication technique adopted. A detailed procedure for microdevice fabrication is presented elsewhere (Paiè et al. 2014; Prabhakar et al. 2015). SU8-2100 photoresist was spin-coated on the Silicon wafer at 3000 rpm to obtain the desired depth of 100 μm (±5 μm). This was followed by pre-baking, exposure to UV light and post-baking. The silicon wafer was then developed to obtain the final SU8 mold structure with design engraved on it. Once the silicon mold was prepared, a 10:1 mixture (w/w) of PDMS and curing agent was prepared and poured over the mold. The silicon mold, now with PDMS layer on it, was then cured at 70 °C for 1 h. Subsequently, PDMS was peeled off from the silicon mold structure, and holes were punched at the reservoir locations to facilitate fluid flow. The PDMS chip was bonded to a glass plate with a thin (~6 μm) intermediate adhesive layer of PDMS (Tripathi et al. 2013, 2015; Prabhakar et al. 2015). Finally, the inlet and outlet tubes were attached to the reservoir holes.

3.2 Experimental setup

Two different experimental setups are used to confirm 3D hydrodynamic flow focusing. The first experimental setup consists of a syringe pump for introducing the sample
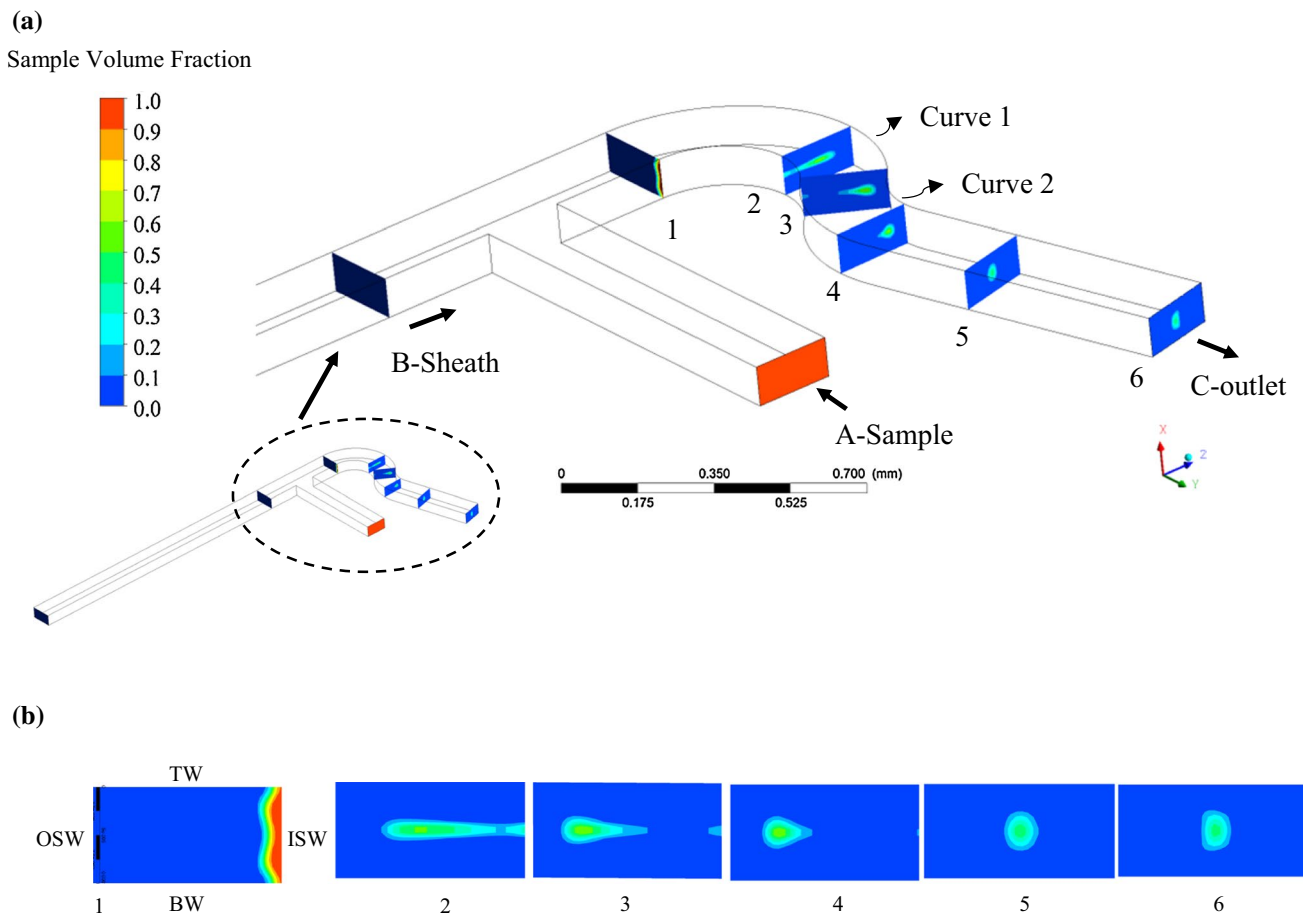
(a)

Sample Volume Fraction

(b)

Fig. 1 **a** Proposed microdevice for obtaining 3D focusing of the sample fluid. **b** CFD simulation showing volume fraction of the sample fluid at various cross sections along the microchannel length (*BW* bottom wall, *TW* top wall, *OSW* outer side wall, *ISW* inner side wall)
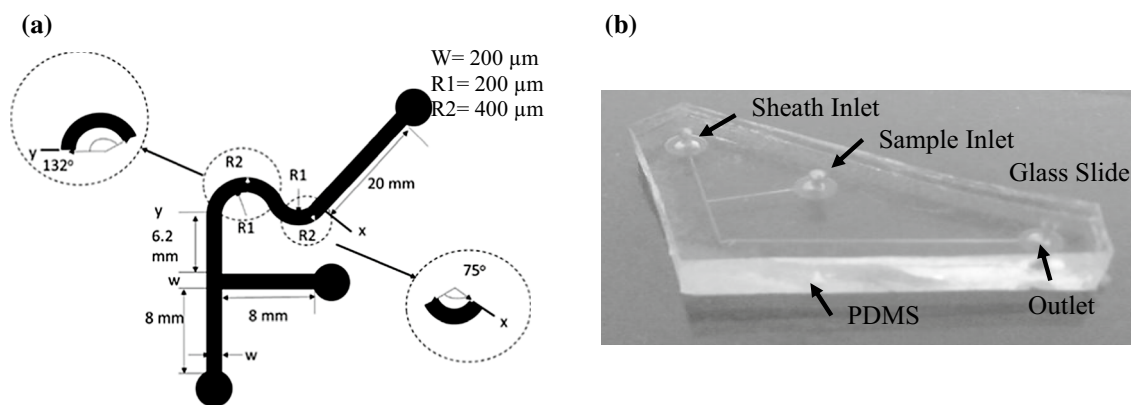
(a)

W= 200 μm
R1= 200 μm
R2= 400 μm

(b)

Fig. 2 **a** Schematic showing the geometrical details of the microchannel. **b** Photograph of the microdevice

fluid (diluted blood), a peristaltic pump with a damper for sheath flow (saline solution), master flex tubing and connectors. Images and videos were captured using a CCD camera (4× magnification at 25 fps) attached to a microscope. Before starting the experiment, the PDMS device was thoroughly flushed with DIW (deionized water). The syringe was shaken at regular intervals to avoid settling of blood cells, and recording was performed once steady conditions had been attained. Blood samples used in the experiments were obtained from a blood bank. Fresh blood was

Fig. 3 Schematic of the side-view technique employed to detect focusing of blood cells
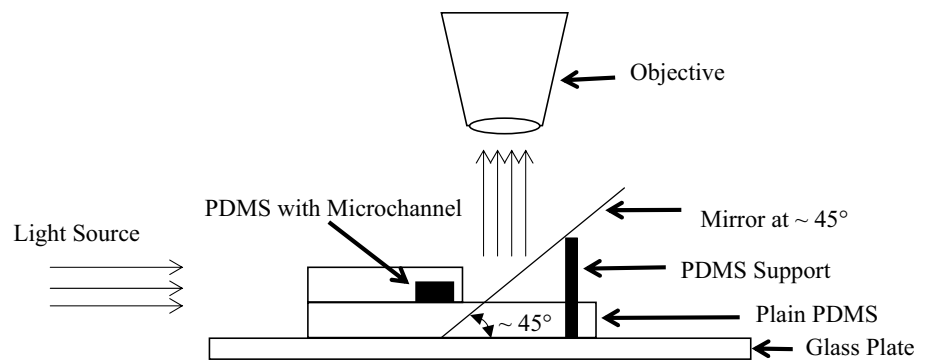
collected from a healthy adult through venipuncture, tested for any communicable diseases and mixed with EDTA solution (anticoagulant). The obtained blood was diluted with physiological saline solution (0.9 % NaCl) to prepare blood samples of 5 % hematocrit level (Tripathi et al. 2013; Kumar et al. 2013; Prabhakar et al. 2015). The second experimental setup is to confirm 3D flow focusing using confocal microscopy, the details are mentioned in Sect. 3.4.

3.3 Detection of blood cell focusing

The microdevice was tested at different flow ratios of sheath/sample. For experiments involving blood as the sample fluid and saline water as the sheath, both vertical and horizontal images were obtained during the experiments. The horizontal focusing images were obtained using the CCD camera attached to the microscope, and for vertical focusing, side-view imaging technique was implemented (Choi and Park 2008; Choi et al. 2010). The side view was obtained to confirm the vertical focusing of the sample. For experiments involving FITC dye and particles, confocal microscopy was employed. The side-view images in these cases were obtained by stacking the XY images, and the detailed procedure is described in Sect. 3.4.

For the experiments adopting blood as sample fluid, a home-made detection system was designed and developed to obtain the side-view images of the microchannels. A schematic illustration of the detection system developed is presented in Fig. 3. As it can be observed from the schematic, the system essentially comprises two PDMS layers, placed one over the other. The top (first) PDMS layer is the one with the design embossed on it. The bottom (second) PDMS layer is a plain layer, i.e., just a layer without any sort of design on it. On the second layer of PDMS, a small mirror is placed at approximately 45° to the horizontal. The small mirror is placed and is held in position with the assistance of a support (PDMS-based support in our case).

The fabrication details of the detection system are as follows. The top (first) PDMS layer (10:1) with the design engraved on it was fabricated as per the procedure described in Sect. 3.1. After curing, this PDMS layer was peeled off from the SU8 mold structure. Holes were punched at the reservoir locations to facilitate fluid flow.

Next, another PDMS layer (20:1), without any sort of design, i.e., the bottom plain layer was fabricated. A mirror was embedded on to this layer at an angle of ~45° to the horizontal. In the next step, the top 10:1 PDMS layer (with the design engraved on it) was bonded on to the second layer, i.e., the bottom plain layer of PDMS (which now has a mirror at one side). The side view of the microchannel through which sample flow occurs can be obtained by projecting a light source as shown in Fig. 3. Therefore, we observed sample flow in the vertical direction and could confirm sample focusing in the vertical direction.

3.4 Detection of FITC dye and particles using confocal microscopy

To obtain additional confirmation of three-dimensional focusing of sample, experiments were conducted using laser scanning confocal microscope (Olympus IX81). The images were processed using software Fluoview FV500. Focusing was observed at a magnification of $10\times$ by placing the microdevice on an inverted microscope. The sample was excited using argon laser over a frequency range of 457–514 nm. One set of flow focusing experiments was carried out using FITC dye, and the other set was carried out using FITC-labeled microparticles based on melamine resin (Sigma-Aldrich). The size of microparticles (6 μm) was chosen so as to mimic the red blood cells (RBCs).

The desired concentration of the sample in different ratios was prepared by diluting the FITC dye using DIW. The particles were diluted with DIW to a desired concentration of 3×10^6 beads/ml, and this corresponds to a dilution ratio of around 200:1. The dye sample concentration was around 60 μg/ml. The experiments were carried out at different flow rates of sample and sheath fluids. The flow rates for experimentation were chosen on the basis of

numerical analysis along with the constraints in bonding strength of the PDMS channel.

After initializing the setup by mounting the sample on the confocal microscope holder and establishing flow using syringe pumps, sufficient time for the establishment of steady flow conditions was provided and images were captured. The total depth of the XY scanning was typically 140 μm with a step size of 2 μm between consecutive images. The images obtained were further processed using ImageJ software. Images generated were imported into the software and were stacked by specifying the depth between consecutive images as 2 μm.

3.5 Numerical methodology

Computational fluid dynamics simulations were carried out using ANSYS-FLUENT 14.5. Simulations were performed on a scaled-down three-dimensional model of the fabricated microdevice. The computational domain consists of 593,000 hexahedral cells (mesh size 6 μm × 6 μm). Grid independence tests were performed before finalizing the results. The problem is studied using two different numerical models. Multiphase model with volume of fluid (VOF) method (Wang et al. 2012; Yang and Hsieh 2007) was employed to approximate the flow behavior of sample fluid. Discrete phase model (DPM)-based simulations were performed for particle tracking, i.e., to understand the flow behavior of particles.

For the VOF method, the flow conditions are laminar, incompressible and steady. Velocity inlet boundary condition was set for sample and sheath inlets and pressure outlet at the exit with no-slip boundary condition at walls. Sample's (FITC dye) density and viscosity were set to 1000 kg/m^3 and 0.001 Pa s, respectively. Sheath's density and viscosity were set as 998 kg/m^3 and 0.001 Pa s, respectively. The results obtained with these conditions are shown in Fig. 1. We also tried to numerically assess the behavior of microdevice on employing a fluid with higher viscosity (0.0018 Pa s) and density (1080 kg/m^3) at the sample section. The sample properties assumed (Pries et al. 1992) represent diluted blood (5 % hematocrit) as the sample fluid. The corresponding result is presented in Sect. 4.3 and is shown in Fig. 8a.

The radius and bending angles of curvature 1 and curvature 2 along with the outlet channel were optimized till desired results were obtained. The sample volume fraction can be controlled by setting the velocities of the sample and sheath. In this work, a segregated solver and an implicit technique are used to resolve the algebraic equations. The governing equations were solved by choosing SIMPLE scheme for pressure–velocity coupling. Second-order upwind discretization for both momentum and volume fraction and PRESTO for pressure is chosen as the

solution method. The residual convergence criteria were set to 1×10^{-9}.

3.6 Particle focusing and tracking using DPM method

To trace the particles flowing in the microchannel, discrete phase model (DPM) provided by ANSYS 14.5 is employed. The discrete phase model (DPM) follows Euler–Lagrange approach to track the particle. ANSYS-FLUENT predicts the trajectory of a discrete phase by integrating the force balance on the particle in a Lagrangian reference frame. The particles are introduced along with the sample, and their motion is studied. The hydrodynamic focusing phenomena are observed by tracking the particle path. To begin with, the steady solution is obtained by solving the continuous phase. Subsequently, the discrete phase is included in the model by defining the initial position, velocity and size of the particles. The discrete phase model is enabled, and the interaction with the continuous phase option is also enabled. The details for the DPM settings are given in Table 1.

Two different approaches were used in the DPM modeling. In the first approach, DPM model was used in a single-phase fluid to approximate the flow behavior of FITC-labeled microparticles. The experiments on FITC-labeled particles were carried out by employing DIW as the sheath fluid, and microparticles diluted with DIW as sample fluid. The corresponding simulation results are shown in Fig. 4. We have also attempted to simulate blood cells using a second approach, i.e., DPM for multiphase fluid using a mixture model (the details are provided in Table 1). The corresponding numerical simulation results are shown in Fig. 8b and discussed in Sect. 4.3.

4 Proof of the proposed design

4.1 Numerical verification of the design

In order to prove the above design, numerical simulations were carried out. Figure 1 is obtained using the multiphase volume of fluid method. In Fig. 1, 'A' is the inlet for the sample fluid (volume fraction of sample is unity—shown by orange color) and 'B' is the inlet for the sheath fluid (volume fraction of sample is zero—shown by blue color). The device has bends at two locations, designated as curve 1 and curve 2. The sample/sheath is tracked at six different critical locations along the cross-sectional plane; the results are presented through the contours of volume fraction. In Fig. 1, the sample velocity is 0.1 m/s (0.12 ml/min) and sheath is 2.8 m/s (3.2 ml/min).

Plane 1 shows sample interaction with sheath before the two streams enter the first curvature. At plane 2 (located at the center of the first curvature), the sample is seen to

Fig. 4 Simulation result: particle focusing using DPM sample velocity 0.1 m/s (0.12 ml/min) and sheath at 2.8 m/s (3.2 ml/min)
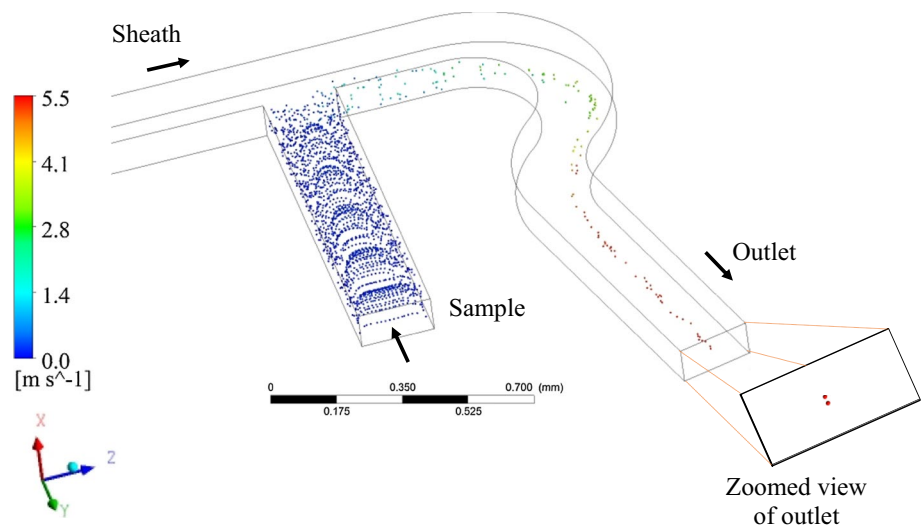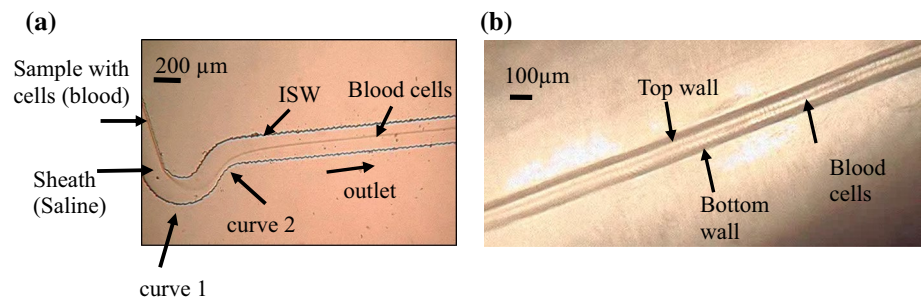

Fig. 5 Experimental result of flow focusing using cells, sample and sheath flow rate of 0.12 and 1.8 ml/min, respectively: **a** horizontal focusing and **b** vertical focusing of cells

spread horizontally (more so on the inner side). As shown later in Sect. 5, this is owing to secondary flows generated due to curvature effects. As the fluid moves further along curve 1, sample starts detaching from the inner side wall (ISW), as evident from the contours in plane 3. Next the sample/sheath fluids enter curve 2. This curve is of the same dimensions as curve 1 but placed inverted in orientation to curve 1. At plane 4 (located at the outlet of the second curvature), the sample is completely detached from ISW. This is because of the effect of centrifugal force, which facilitates the sample to detach from ISW. Further downstream of curve 2 at plane 5 (located 200 μm from plane 4), the sample is centrally focused between the outer and inner side walls. Focusing in a further downstream plane (plane 6, located 600 μm from plane 5) has also been checked for the sake of completeness and also allowing space for mounting of a sensor. Note that the sample is completely surrounded by the sheath fluid, therefore three-dimensional hydrodynamic focusing has been achieved in the simulations.

To further verify the design, 3D flow focusing of particles using the DPM-single phase model as described in Sect. 3.6 was carried out. Figure 4 shows the trajectory of particles flowing in the microchannel. The velocity of the

particles is indicated by the legend colors. After the first curvature, the particles are focused in the vertical direction (due to Dean vortices). This observation is evident from Fig. 1. The second curvature enables horizontal focusing and aids in centering the focused stream. The color change in the particle indicates that the particles are at a higher velocity at the outlet due to the combined flow rate (of sample and sheath). Near the outlet of the microchannel, particles travel with a uniform velocity of 5.5 m/s. The particles seem to form a single file at the outlet of the microchannel, thereby confirming 3D focusing of particles; however, the presence of two to three 6 μm particles at a cross section is noticed for the conditions employed in our device.

4.2 Experimental verification of the design

The design is further verified through experiments as discussed in this section. Experiments were carried out with blood cells as sample, as described in Sect. 3.2.

The sample fluid employed is blood cells (hematocrit 5 % and sheath is saline). Figure 5a shows the image of the fabricated channel; focusing takes place as observed from the top view. Sample flow rate is 0.12 ml/min (0.1 m/s) and sheath flow velocity is 1.8 ml/min (1.6 m/s) for this

Fig. 6 Experimental results using confocal microscope. **a** *x–y* image showing focusing of FITC-labeled particles for sample flow rate of 0.12 ml/min and sheath (DIW) flow rate of 3.2 ml/min. **b–e** Cross-sectional image at section *A–A* in (**a**) for different flow rates of FITC-labeled particles/dye and sheath. Note that section *A–A* approximately corresponds to plane 5 in Fig. 1. The flow rates of FITC-labeled particles and sheath, respectively, are **b** 0.12 and 3.2 ml/min; **c** 0.12 and 2.4 ml/min. The flow rates of FITC-labeled dye and sheath, respectively, are **d** 0.12 and 2.4 ml/min; **e** 0.12 and 3.2 ml/min
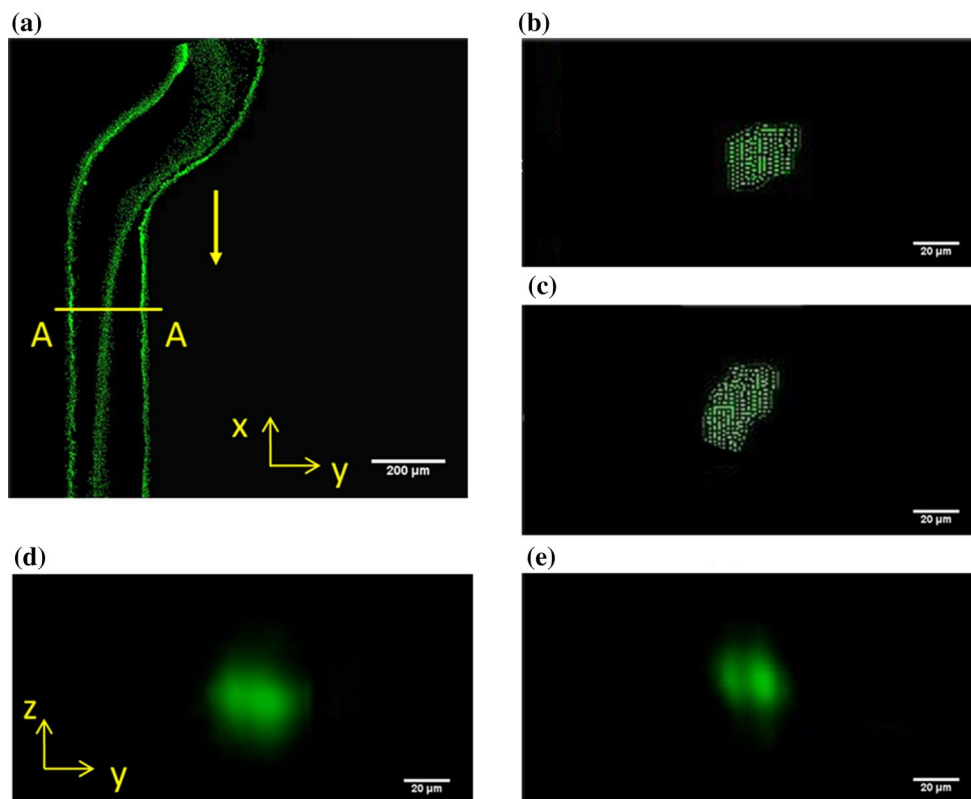
measurement. The blood cells can be seen to be centrally focused between the outer and inner side walls. Figure 5b shows the side view of the microchannel, and the cells are clearly seen to be focused between the top and bottom walls of the microchannel, confirming 3D hydrodynamic focusing.

Further experiments were conducted using confocal microscope on the microchannel as per the procedure described in Sect. 3.4. Figure 6a shows the top view of the microchannel with particles along the *xy* plane. The figure also shows overlapped images of the particles (or dye) in the cross section of the design at the desired location of interest (plane A–A). It is observed from Fig. 6a that horizontal focusing of the sample takes place and the focusing continues up to considerable distance along the microchannel length with minimal dispersion. Section A–A, which is approximately 200 μm from the end of the second curve in the design, represents the plane at which the cross-sectional images of the samples are obtained and are shown in Fig. 6b–e. It can be clearly observed from Fig. 6 that sample focusing takes place in the horizontal as well as vertical planes of the microdevice. Comparison of focusing in Fig. 6 and numerical simulation results in Fig. 1 reveals that there is a good correlation between the experimental observations and the numerical results. It can be noted from Fig. 6 that concentration of sample can be thought as being focused in a region enclosing a circle of diameter

approximately 30 μm. The challenge lies in reducing the focused region further.

In order to better estimate the location and width of the focused region, confocal microscopy-based images were converted into gray scale. Based on the intensity values obtained at each pixel location, the intensity profiles were plotted along the width (*y*) and depth (*z*) wise directions. The intensity profiles also reveal the expected focusing outcome of the sample, which is concentrated at the center of the channel. Based on the intensity profiles obtained, the mean position around which the focusing is concentrated is calculated. The intensity profile was derived using the grayscale images, and the mean lateral position of the focused sample was calculated as $y_m^* = \frac{1}{w} \sum_{i=1}^{n} \frac{y_i I_i}{I_i}$ and $z_m^* = \frac{1}{h} \sum_{i=1}^{n} \frac{z_i I_i}{I_i}$ along the *y* (width) and *z* (depth) directions respectively, where y_i and z_i are the pixel locations in the *y* and *z* directions, I_i represents the intensity value at a particular pixel and '*w*' and '*h*' represents the width and the depth of the microchannel, respectively. The values of normalized standard deviation have also been provided, and these are represented as y_σ^* and z_σ^* along width and height of the microchannel respectively.

Figure 7 provides the intensity profile of the focused sample in the cross-sectional plane. Figure 7c shows the overlaid intensity profile of VOF simulation with that of the experimental result on FITC dye (at the same flow

Fig. 7 Intensity profiles for sample and sheath flow rate of 0.12 and 3.2 ml/min, respectively (*gray values* at arbitrary units). **a** FITC-labeled particles along *z*-direction, **b** FITC-labeled particles along *y*-direction, **c** FITC dye (experimental) and simulation result, along *z*-direction **d** FITC dye (experimental) and simulation result, along *y*-direction. (The *grayscale* values are at arbitrary units. The intensity (*gray scale*) values of numerical results for Fig. 7c, d have been scaled to those of the intensity value of experimental results)
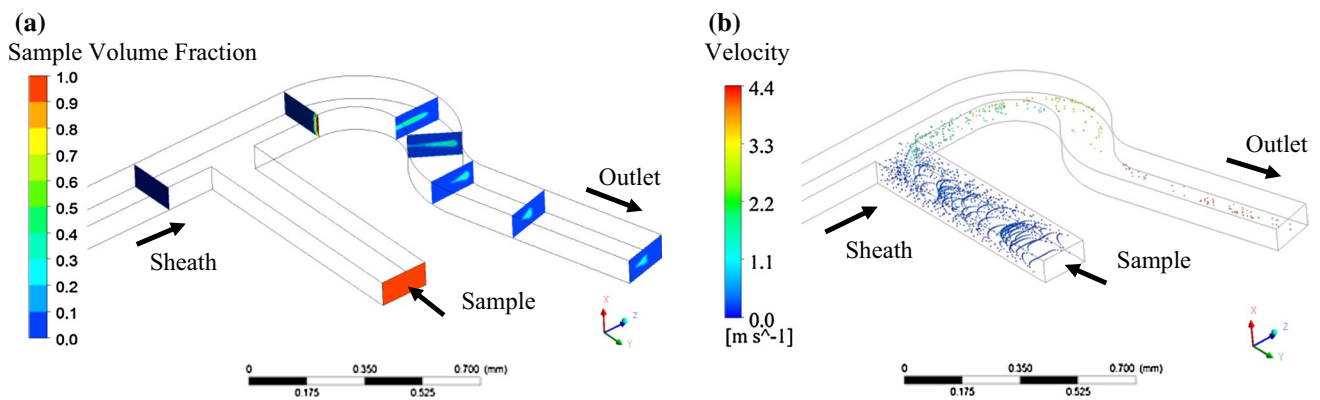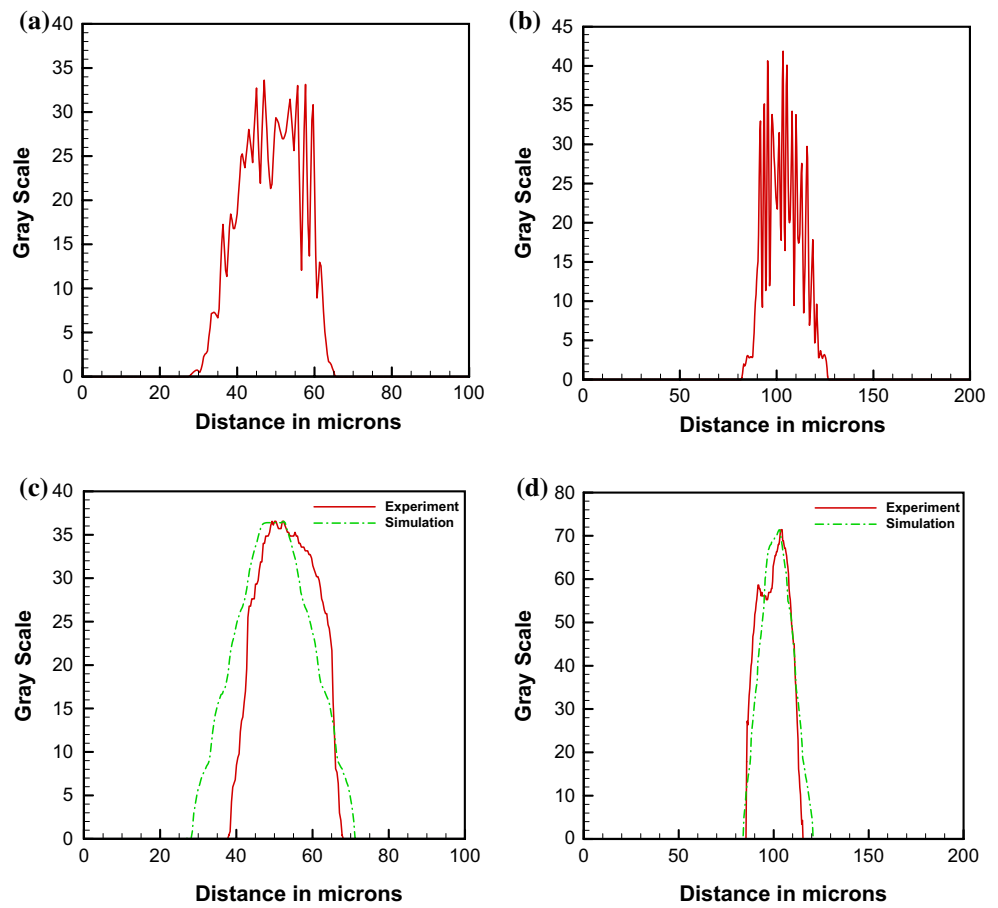

Fig. 8 Simulation result. **a** VOF result. **b** Particle tracking using DPM for sample flow at 0.12 ml/min and sheath flow 1.8 ml/min

conditions). It can be observed from this figure that experimental result on FITC dye, and VOF simulation are in good agreement. Table 2 provides the mean lateral positions for the samples shown in Fig. 6b–e. It can be observed from the values of the normalized mean positions obtained that the concentration of the sample with high intensity is always very close to the center of the microchannel with decreasing intensity as one moves outward from the center.

Also, the normalized standard deviation values show that the sample is concentrated in a region very close to the center of the microchannel.

4.3 Comparison of experimental and numerical results

A qualitative comparison of experimental and numerical results is presented in this section. The numerical validation

Table 1 DPM settings used to obtain particle tracking in the microdevice

Model	DPM-single phase	DPM-mixture
Solver	Pressure	Pressure
Materials	Sheath—density 998 kg/m^3 and viscosity 0.001 Pa s	Sample—density 1080 kg/m^3 and viscosity 0.0018 Pa s; sheath—density 998 kg/m^3 and viscosity 0.001 Pa s
Phases	One	Two
Injection properties	Injection surface-sample; diameter of particle—6 μm; initial velocity—0 m/s; uniformly injected; mass = 1e−8 kg/s; density of particles—1080 kg/m^3	
DPM settings	Max no. of steps 50,000; step length factor 5; interaction with continuous phase with unsteady particle tracking; spherical drag law and physical models-virtual mass force, Saffman lift force	
Boundary conditions	Velocity condition for sample and sheath and outlet pressure—zero; DPM BC sample—escape, sheath—reflect, outlet—escape	
Solution method	Pressure velocity coupling, scheme-coupled; discretization—pressure-presto, momentum—second-order upwind, volume fraction—quick (DPM-mixture)	

Table 2 Normalized mean position and standard deviation of the focused sample fluid

Sample	y_m^*	y_σ^*	z_m^*	z_σ^*
FITC dye (0.12, 2.4 ml/min)	0.53075	0.06755	0.4528	0.1111
FITC dye (0.12, 3.2 ml/min)	0.5012	0.05025	0.5256	0.089
FITC particles (0.12, 2.4 ml/min)	0.471	0.05025	0.5649	0.1188
FITC particles (0.12, 3.2 ml/min)	0.5185	0.0635	0.4863	0.0967

of the proposed design is already shown in Figs. 1, 4 and 6, where the sample velocity was set as 0.1 m/s (0.12 ml/min) and sheath at 2.8 m/s (3.2 ml/min). The numerical study was carried out mainly to understand the flow behavior of FITC dye and particles. However, in this section we tried to assess the validity of numerical results with those of the experimental observations on blood cells.

Figure 8 presents the simulation results (both VOF and DPM—particle tracking) under the same flow conditions as in Fig. 5. However, in this case, DPM-mixture model was employed for particle tracking (Table 1). The properties chosen for this case, sample (blood Hct 5 %), the density and viscosity were set to 1080 kg/m^3 and 0.0018 Pa s. Sheath's density and viscosity were set as 998 kg/m^3 and 0.001 Pa s. On comparison, it is seen that the simulation results closely follow the experimental results shown in Fig. 5. For example, at plane 2, spreading of cells (horizontal spreading) can be observed in both the experimental figure and simulation result. Similarly, the trajectory of cells at the two curves compares well with each other. It is also seen that the sample fluid is well focused at the outlet (Fig. 8a, b) and a group of cells are flowing centrally across the outlet cross section of the microchannel.

Further, we compare the focused area of the sample flow. The focused area in the cross-sectional plane at a distance 200 μm from curve 2 for conditions specified in Fig. 5 is 280 μm^2; the corresponding area from the simulation result is 299 μm^2 (Fig. 8a).

Our experiments and subsequent data analysis provide some important observations. If the sample is prepared at the appropriate concentration levels and the flow visualization is carried at higher magnification, the possibility of getting close to a single cell focusing in a region concentrated at the center of the channel cross section is achievable with the proposed design. We have validated this proposition numerically by lowering the sample inlet concentration, which results in cells being focused in a single file.

5 Discussion

In this section, we provide brief discussion on the working principle of the proposed microdevice. The magnitude of forces acting on particles as they flow through the microdevice is also calculated and discussed.

5.1 Generation of secondary forces in the microdevice

Figure 9 provides details about the secondary forces generated through flow in the microchannel. To gain further insight into this phenomenon, helicity contours at different cross-sectional planes shown in Fig. 1 are considered. Helicity provides information of the vorticity component aligned along the fluid stream. It can be defined as the dot product of vorticity and velocity vector, $H = (\nabla \times V).V$. Secondary flows can be characterized using the Dean number which is defined as $De = Re\sqrt{\frac{D_h}{R_c}}$, where Re is the Reynolds number, D_h is the hydraulic diameter of the microchannel and R_c is the mean radius of the curvature of the microchannel. It is known that high Dean number results in increment of the number of vortices (Bara et al. 1992; Fellouah
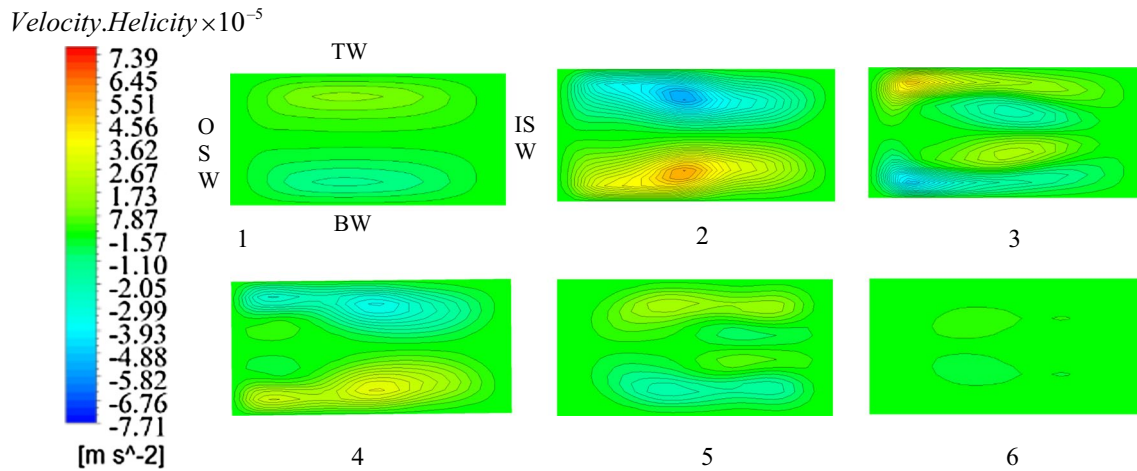
Fig. 9 Generation of secondary flows in the microchannel shown through contours of helicity at sample and sheath flow rate of 0.12 and 3.2 ml/min, respectively (*BW* bottom wall, *TW* top wall, *OSW* outer side wall, *ISW* inner side wall)

Table 3 Flow parameters considered for particle force analysis

w and h (µm)	D_h (µm)	R_c (µm)	d_p (µm)	ρ_p (kg/m³)	ρ_f (kg/m³)	μ_f (Pa s)
200 and 100	133.33	300	6	1080	998	0.001

Table 4 Comparison of forces acting on particles

u_p (m/s)	Re_f	De	$U_\mathcal{D}$ (m/s)	F_{centg} (N)	F_L (N)	F_{netg} (N)	F_D (N)
2.8	372.58	248	1.44	2.42×10^{-10}	1.14×10^{-9}	9.1×10^{-14}	8.16×10^{-8}
1.1	146.37	97.6	0.315	3.74×10^{-11}	1.76×10^{-10}	9.1×10^{-14}	1.78×10^{-8}
2.2	292.74	195	0.97	1.5×10^{-10}	7.04×10^{-10}	9.1×10^{-14}	5.51×10^{-8}
5.5	731.86	488	4.34	9.35×10^{-10}	4.4×10^{-9}	9.1×10^{-14}	2.45×10^{-7}

et al. 2006; Ha et al. 2014). If the curvature is properly controlled, the additional vortices generated may assist flow focusing of the sample fluid. Herein, the presence of vortex can be seen near the top and bottom walls of the microchannel at plane 1. At plane 2, counter-rotating vortices (blue color and orange color signify rotational directions) are observed, which assist in focusing the sample fluid in the vertical direction.

At plane 3, four counter-rotating vortices are observed and the sample fluid moves toward the OSW of the microchannel. Two additional small vortices are generated at plane 4, and these additional vortices aid the centering of the sample fluid in the microchannel. These observations of four vortices and their role in aiding the sample focusing have also been reported by other researchers (Bara et al. 1992; Ha et al. 2014). As the flow progresses toward the outlet of the microchannel, the vortex strength subsides, but the sample core at the central region of the microchannel remains unaffected. At plane 5, the sample is found to be completely focused. The helicity contours reveal the absence of Dean vortices at the outlet, which can be seen at plane 6.

5.2 Force analysis on particles/cells

In order to study the behavior of particles in curved microchannels, a force analysis study is imperative. Particles flowing through curved microchannels are subjected to inertial effects, viscous drag, net gravitational forces, lift forces and net centrifugal forces (Mao et al. 2009). These forces have been calculated as discussed in (Appendix). In our analysis, we consider four different cases to estimate values of the forces generated. Table 3 shows the parameters used for force analysis. The calculated values of various forces are presented in Table 4. In all the cases, it is clearly observed that lift and viscous drag is dominant over other forces. This confirms that the particles follow the streamlines and focusing of particles takes place as desired. We have also confirmed that the drag force is dominant for a large range of particle sizes.

6 Advantages of the proposed microdevice

The unique features of the present microdevice are as follows: In general, designs presented in the literature involve complex fabrication process with multiple layers of PDMS, whereas in our design, only a single layer of PDMS is used to fabricate the microchannel. In the proposed microdevice, only a single sheath inlet is required as input, whereas existing flow focusing designs involve more than one sheath inlets, thereby increasing the complexity of their design. Reduction in the number of inputs is a significant improvement considering that cost reduction occurs with reduction in additional pumps.

An additional benefit in our design is the control in locating the sample stream, which allows better centralized focusing. Further, as demonstrated in Sect. 4.2, this central line focusing is not restricted to a narrow range of flow rates of sheath and sample fluid, rather centralized focusing is achieved over a wide range of parameters. In comparison with other designs, our microchannel is provided with curves which change course in opposite directions. This alternate curvature assists in placing detection system in parallel quite easily in comparison with systems where curvature is unidirectional. Compared with curved microchannels, straight microchannels that are capable of sample focusing usually require larger microchannel length to achieve focusing. Therefore, by employing curved microchannels, as in our case, would result in compact microdevices and may also lead to lower power consumption to operate the microdevice. The importance of employing curves and making the microdevice compact has recently been emphasized in DiCarlo (2009). The flow rate range in which the microdevice performs very effectively is with sample flow rate of 0.08–0.12 ml/min and sheath flow rate of 1–3.2 ml/min. This ensures continuous functioning of the device with desired outcome of 3D focusing without leakage issues (Ha et al. 2014). Finally, the capability of the design to focus different samples, including dye, particles and cells has been demonstrated, suggesting that a single microdevice can cater to all types of focusing needs.

7 Conclusion

In the present work, we demonstrated a novel way of 3D hydrodynamic focusing by employing alternate curves, single sheath inlet, exploiting secondary forces and centrifugal effects. The results obtained establish that the sample is well-focused three-dimensionally at the center of the microchannel. Both horizontal and vertical focusing is achieved by optimizing the curvature geometry employed in the design of the microchannel. Successful functioning of the microdevice has been demonstrated both numerically and experimentally.

This microdevice can be fabricated easily on a single layer of PDMS without necessity of costly and complex fabrication techniques. The proposed microdevice provides excellent sample control over a wide range of flow parameters. We demonstrate efficient working of the microdevice by focusing biological cells (blood cells) in three dimensions. This microdevice can be employed for focusing dye, particles and cells and can therefore cater to various focusing needs in optical waveguides, flow switches, microflow cytometry and other real-life applications.

Appendix

This section outlines the force analysis formulation used in Sect. 5.2:

(a) Centrifugal force: Due to the presence of a curvature, the particles are subjected to a net centrifugal force which is directed away from the center of curvature (Fig. 10a). This force is given by Eq. 1 (refer nomenclature for symbols)

$$F_{centg} = \frac{\pi d_p^3 (\rho_p - \rho_f) u_p^2}{6R} \tag{1}$$

(b) Net gravitational force: Particle is subjected to a net gravitational force. Gravitational force acts downward and a buoyant force acts upward due to the sheath fluid (Fig. 10b). It is given by Eq. 2.

$$F_{netg} = \frac{\pi d_p^3 (\rho_p - \rho_f) g}{6} \tag{2}$$

(c) Viscous drag force: This drag force is due to the rotational Dean flow and is approximated as Stokes drag (the relative Reynolds number is small). For large Dean number, Stokes drag due to secondary flow becomes dominant (DiCarlo et al. 2008). This force causes the particle to move along the streamlines. It sweeps the particles in a perpendicular direction to the main flow and then accelerates the particles to the end of microchannel. The direction of this force is dependent on the position of the particle in the microchannel as shown in Fig. 10c. The two counter-rotating vortices are shown

Fig. 10 Representation of forces acting on particles. **a** Centrifugal. **b** Net gravitational. **c** Dean drag. **d** Net lift force. **c**, **d** is adapted from Mao et al. (2009) and DiCarlo (2009), respectively.
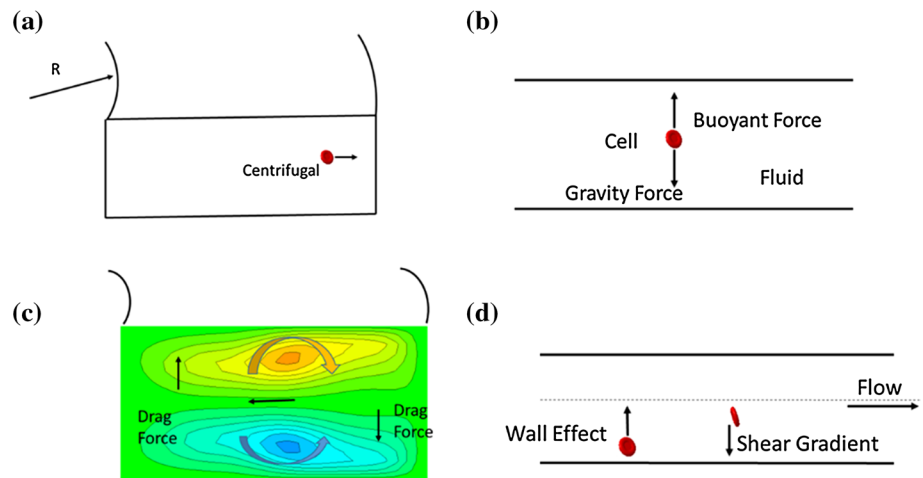
in this figure, and the arrow signifies the direction of the force.

$$F_D = 3\pi \mu_f d_p U_D \tag{3}$$

where U_D is average Dean flow velocity or local secondary flow velocity, which is given by (Bhagat et al. 2008)

$$U_D = 1.8 \times 10^{-4} De^{1.67} \tag{4}$$

(d) Lift force: The inertial lift forces are responsible for the lateral migration of particles across the flow streamlines. The parabolic velocity profile in flow produces a shear-induced inertial lift force that drives particles away from the microchannel center toward microchannel walls. As particles migrate closer to the channel walls, an asymmetric wake induced around particles generates a wall-induced lift force driving these particles away from the walls (DiCarlo et al. 2008; refer Fig. 10d). The net lift force acting on a neutrally buoyant particle can be estimated by Eq. (5) (Kemna et al. 2012).

$$F_L = \frac{2\rho_f U_D^2 d_p^4}{D_h^2} \tag{5}$$

References

Amini H, Sollier E, Masaeli M, Xie Y, Ganapathysubramanian B, Stone HA, Di Carlo D (2013) Engineering fluid flow using sequenced microstructures. Nat commun 4:1826

Anna SL, Bontoux N, Stone HA (2002) Formation of dispersions using "flow focusing" in microchannels. Appl Phys Lett 82:3

Bara B, Nandakumar K, Masliyah JH (1992) An experimental and numerical study of the dean problem: flow development towards two-dimensional multiple solutions. J Fluid Mech 244:339–376

Bhagat AAS, Kuntaegowdanahalli SS, Papautsky I (2008) Continuous particle separation in spiral microchannels using dean flows and differential migration. Lab Chip 8:1906–1914

Blonski S, Domagalski P, Dziubinski M, Kowalewski TA (2011) Selective seeding in micro-PIV. Arch Mech 63(2):163–182

Brown M, Vestad T, Oakey J, Marr DWM (2006) Optical waveguides via viscosity-mismatched microfluidic flows. Appl Phys Lett 88:134109

Chang CC, Huang ZX, Yang RJ (2007) Three-dimensional hydrodynamic focusing in two-layer polydimethylsiloxane (PDMS) microchannels. J Micromech Microeng 17:1479–1486

Chiu YJ, Cho SH, Mei Z, Lien V, Wu TF, Lo YH (2013) Universally applicable three-dimensional hydrodynamic microfluidic flow focusing. Lab Chip 13:1803–1809

Choi S, Park JK (2008) Mirror-embedded microchannel for three-dimensional measurement of particle position. Appl Phys Lett. 93(19):191909

Choi S, Kim SH, Park JK (2010) Optical path-length modulation for three-dimensional particle measurement in mirror-embedded microchannels. Lab Chip 10:335–340

Chung S, Park SJ, Kim JK, Chung C, Han DC, Chang JK (2003) Plastic microchip flow cytometer based on 2- and 3-dimensional hydrodynamic flow focusing. Microsyst Technol 9:525–533

de Mello AJ, Edel JB (2007) Hydrodynamic focusing in microstructures, improved detection efficiencies in subfemtoliter probe volumes. J Appl Phys 101:084903

DiCarlo D (2009) Inertial microfluidics. Lab Chip 9:3038–3046

DiCarlo D, Edd JF, Irimia D, Tompkins RG, Toner M (2008) Equilibrium separation and filtration of particles using differential inertial focusing. Anal Chem 80:2204–2211

Fellouah H, Castelain C, Ould El Moctar A, Peerhossaini H (2006) A criterion for detection of the onset of dean instability in Newtonian fluids. Eur J Mech B Fluids 25:505–531

Ha BH, Lee KS, Jung JH, Sung J (2014) Three-dimensional hydrodynamic flow and particle focusing using four vortices dean flow. Microfluid Nanofluid 17:647–655

Howell PB Jr, Golden JP, Hilliard LR, Erickson JS, Mott DR, Ligler FS (2008) Two simple and rugged designs for creating microfluidic sheath flow. Lab Chip 8:1097–1103

Kemna EWM, Schoeman RM, Wolbers F, Vermes I, Weitz DA, Berg A (2012) High-yield cell ordering and deterministic cell-in-droplet encapsulation using Dean flow in a curved microchannel. Lab Chip 12:2881–2887

Kennedy MJ, Stelick SJ, Perkins SL, Cao L, Butt CA (2009) Hydrodynamic focusing With a microlithographic manifold: controlling the vertical position of a focused sample. Microfluid Nanofluid 7:569–578

Knight JB, Vishwanath A, Brody JP, Austin RH (1998) Hydrodynamic focusing on a silicon chip: mixing nanoliters in microseconds. Phys Rev Lett 80:17

Kumar N, Prabhakar A, Tikekar M, Singh SG, Agrawal A (2013) Blood flow in non—circular microchannel under pulsating condition. Int J Micronano Scale Transp 4(1):33–50

Lee GB, Hung CI, Ke BJ, Huang GR, Hwei BH, Lai HF (2001a) Hydrodynamic focusing for a micromachined flow cytometer. J Fluids Eng 123:672–679

Lee GB, Hung CI, Ke BJ, Huang GR, Hwei BH (2001b) Micromachined pre-focused 1 × N flow switches for continuous sample injection. J Micromech Microeng 11:567–573

Lee GB, Lin CH, Chang SC (2005) Micromachine-based multichannel flow cytometers for cell/particle counting and sorting. J Micromech Microeng 15:447–454

Lee GB, Chang CC, Huan SB, Yang RJ (2006) The hydrodynamic focusing effect inside rectangular microchannels. J Micromech Microeng 16:1024–1032

Lee MG, Choi S, Park JK (2009) Three-dimensional hydrodynamic focusing with a single sheath flow in a single-layer microfluidic device. Lab Chip 9(21):3155–3160

Lin SC, Yen PW, Peng CC, Tung YC (2012) Single channel layer, single sheath-flow inlet microfluidic flow cytometer with three-dimensional hydrodynamic focusing. Lab Chip 12:3135–3141

Mao X, Waldeisen JR, Juluri BK, Huang TJ (2007) Microfluidic drifting—implementing three-dimensional hydrodynamic focusing with a single-layer planar microfluidic device. Lab Chip 7:1303–1308

Mao X, Waldeison JR, Huang TJ (2009) Single-layer planar on-chip flow cytometer using microfluidic drifting based three-dimensional (3D) hydrodynamic focusing. Lab Chip 9:1583–1589

Paiè P, Bragheri F, Vazquez RM, Osellame R (2014) Straightforward 3D hydrodynamic focusing in femtosecond laser fabricated microfluidic channels. Lab Chip 14(11):1826–1833

Prabhakar A, Kumar YVBV, Tripathi S, Agrawal A (2015) A novel, compact and efficient microchannel arrangement with multiple hydrodynamic effects for blood plasma separation. Microfluid Nanofluid 18(5–6):995–1006

Pries AR, Neuhaus D, Gaehtgens P (1992) Blood viscosity in tube flow: dependence on diameter and hematocrit. Am J Physiol Heart Circ Physiol 263(6):H1770–H1778

Simonnet C, Groisman A (2006) High-throughput and high-resolution flow cytometry in molded microfluidic devices. Anal Chem 78:5653–5663

Stiles T, Fallon R, Vestad T, Oakey J, Marr DWM, Squier J, Jimenez R (2005) Hydrodynamic focusing for vacuum-pumped microfluidics. Microfluid Nanofluid 1:280–283

Sundararajan N, Pio MS, Lee LP, Berlin AA (2004) Three-dimensional hydrodynamic focusing in polydimethylsiloxane (PDMS) microchannels. J. Electromech S 13:559–567

Tripathi S, Prabhakar A, Kumar N, Singh SG, Agrawal A (2013) Biomed Microdevices 15(3):415–425

Tripathi S, Chakravarty P, Agrawal A (2014) On non-monotonic variation of hydrodynamically focused width in a rectangular microchannel. Curr Sci 107(8):1260–1274

Tripathi S, Kumar YVBV, Prabhakar A, Joshi SS, Agrawal A (2015) Performance study of microfluidic devices for blood plasma separation—a designer's perspective. J Micromech Microeng 25(8):084004

Wang YQ, Wang JY, Chen HL, Zhu ZC, Wang B (2012) Prototype of a novel micro-machined cytometer and its 3D hydrodynamic focusing properties. Microsyst Technol 18:1991–2001

Yang AS, Hsieh WH (2007) Hydrodynamic focusing investigation in a micro-flow cytometer. Biomed Microdevices 9:113–122